Mechatronics 23 (2013) 1163–1170

Contents lists available at ScienceDirect

Mechatronics

journal homepage: www.elsevier.com/locate/mechatronics

Modeling and experimental validation of new two degree-of-freedom piezoelectric actuators

W.M. Chen, T.S. Liu *

Department of Mechanical Engineering, National Chiao Tung University, Hsinchu 30010, Taiwan, ROC

ARTICLE INFO

Article history:
Received 4 October 2012
Accepted 3 October 2013
Available online 31 October 2013

Keywords:
Piezoelectric actuator
Piezoelectric buzzer
Rotation
2-DOF
Dry friction
Translation

ABSTRACT

This study presents innovative two-degree-of-freedom piezoelectric actuators, which apply piezoelectric buzzers to play as a driving source. Under piezoelectric force and dry friction, the piezoelectric actuators not only can move in the *Z*-axis direction, but also rotate along the *Y*-axis. The *Z*-axis displacement can reach 62 mm and the rotation angle along the *Y*-axis can reach 270°. Compared with the literature, this innovative piezoelectric actuator design easily and rapidly achieves one degree-of-freedom translation and one degree-of-freedom rotation. Equations of motion are derived based on piezoelectric properties and Newton's law. Two types of actuators are created in this study. In the first type, centers of two piezoelectric buzzers are attached to an arm while in the other type each rim of two piezoelectric buzzers is attached to the arm. Experimental results are compared with theoretical results. According to experimental results, the present actuator can accomplish the translational velocity of 21 mm/s, angular velocity of 3.72 rad/s, and 2.32 mN in force. This study presents a piezoelectric actuator capable of both translation and rotation, which is rare in the literature.

1. Introduction

With the development of science and technology in various technical fields, such as aerospace, optics, electronics, and medical engineering, high-precision actuators are required [1–6]. Based on driving principles, types of precision actuators include electrostrictive, magnetostrictive, artificial muscle actuator, shape memory alloy, photostrictive, and mechanochemical acutuators. In the electrostrictive category, piezoelectric actuators are small and possess nanoscale displacement resolution, large driving force, and long stroke [7].

The piezoelectric material used in a piezoelectric actuator comes in types of multilayer, unimorph, bimorph, cylindrical, ring, and disk forms [8–11]. By means of impact drive force, moving bodies can be driven by impulse force [12–16] or by alternate stick and slip method [17–23]. Piezoelectric actuators are employed in precision platforms, atomic force microscopes [24], mobile phones, and digital camera lens drives. To achieve innovative and diverse actuator applications, for which two piezoelectric buzzers subjected to both piezoelectric force and dry friction are employed to undergo *Z*-axis displacement as well as *Y*-axis rotation. Compared with the literature, this innovative piezoelectric actuator design can achieve 1-DOF translation and 1-DOF rotation. Actuator characteristics, including the velocity, angular velocity, and force are measured to validate theoretical models.

2. Two-DOF piezoelectric actuator design and driving process

As depicted in Fig. 1, this study has designed and fabricated two types of actuators: in type-A, two piezoelectric buzzers are fixed at their center points, while in type-B two piezoelectric buzzers are fixed at buzzer rims. Fig. 2 shows that the proposed piezoelectric actuator moves in two DOFs, for which double arrows in Fig. 2 denote translational motion along the *Z* axis and rotation motion along the *Y* axis. The actuator consists of a moving part, a rod, and a base. As depicted in Fig. 3, the moving body comprises a driving part, upper part, lower part, three screws, and three springs. The driving part consists of two piezoelectric buzzers and an arm. Fig. 3 shows an exploded view of the 2-DOF piezoelectric actuator and the dimensions of the two driving part types. The diameter and length of the rod are 3 mm and 70 mm, respectively. The rod and arm are made from carbon fiber material. The upper part, lower part, and base are made from aluminum alloy. The moving body masses of types A and B are 1360 mg and 1320 mg, respectively. Screws between the moving body and the rod are adjusted in order to generate appropriate preloads and dry friction so as to expedite movement. Springs are used on the moving body to maintain a set value for preload and dry friction.

The piezoelectric buzzers play the role as a driving source in this innovative piezoelectric actuator. The positive voltage causes

* Corresponding author.
E-mail address: tsliu@mail.nctu.edu.tw (T.S. Liu).

0957-4158/$ - see front matter © 2013 Elsevier Ltd. All rights reserved.
http://dx.doi.org/10.1016/j.mechatronics.2013.10.002

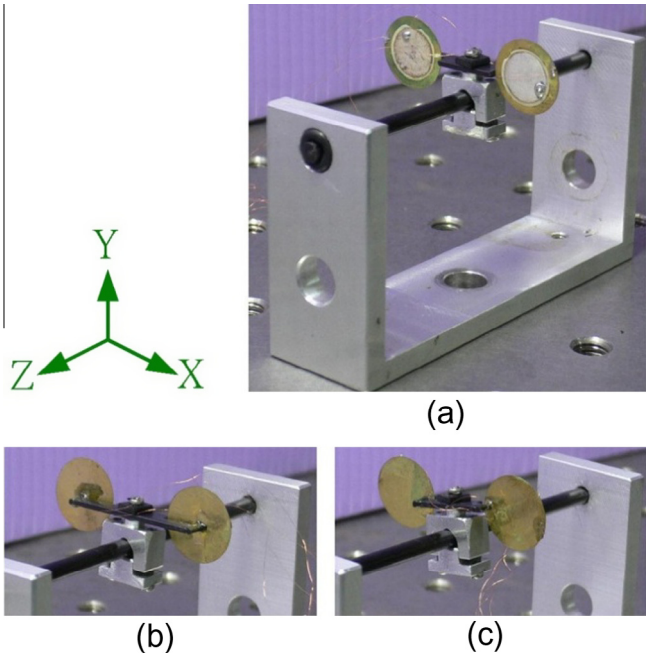

Fig. 1. (a) The present piezoelectric actuator with two types: (b) type-A whose piezoelectric buzzers are attached to the arm at buzzer centers and (c) type-B whose piezoelectric buzzers are attached to the arm at the rim.

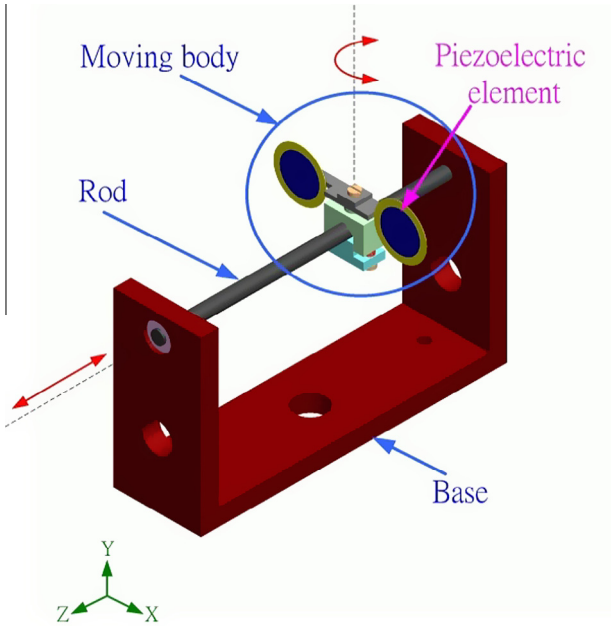

Fig. 2. Two-DOF piezoelectric actuator moving on a rod. Double arrows denote translational DOF along the *Z*-axis and rotational DOF along the *Y*-axis.

the shrinking deformation in the piezoelectric buzzer, while the negative voltage makes the expansion. The deformation speed of the piezoelectric buzzer is adjusted by the duty ratio. Fig. 4 depicts the principle of actuator translation motion along the *Z*-axis direction. The procedure is as follows: (a) the moving body is initially stationary. (b) When both piezoelectric buzzers slowly deform, the summation of the piezoelectric and inertial forces is smaller than the force of dry friction; thus, the moving body does not produce motion and remains in its original location. (c) When both piezoelectric buzzers rapidly deform, the piezoelectric force becomes greater than the friction and triggers motion of the moving body, which moves along the *Z*-axis direction. (d) Finally, both buzzers return to their undeformed state. When steps (a–d) are repeated, the moving body continues to move in the *Z*-axis direction. On the contrary, if both buzzers first rapidly shrink before slowly expand, the moving body moves in opposite directions.

Fig. 5 shows the principle of actuator rotation motion along the *Y*-axis. The axis of the piezoelectric buzzers is parallel to the rod. The principle is described as follows: (a) the moving body is initially stationary. (b) When the top buzzer slowly shrinks while the bottom buzzer slowly expands, the summation of the piezoelectric and inertial forces is too small to move the moving body. (c) When the top buzzer rapidly expands while the bottom buzzer rapidly shrinks, generated torque due to two piezoelectric forces in opposite directions enables the moving body to rotate counterclockwise. On the contrary, if the top buzzer rapidly shrinks while the bottom buzzer rapidly expands, generated torque due to two piezoelectric forces in opposite directions enables the moving body to rotate clockwise. (d) Finally, the two piezoelectric buzzers returned to their undeformed state. When steps (a–d) are repeated, the moving body continues to rotate counterclockwise.

3. Theoretical derivation

This paper presents actuators of two types: type-A, whose piezoelectric buzzers are attached to an arm at both buzzer centers, and type-B, whose piezoelectric buzzers are attached to the arm at buzzer rims. It will be later described in another section on experiments that type-A moves faster than type-B. Therefore, this study only derives deformation equations of type-A piezoelectric buzzers and the dynamic equations of type-A. Based on the deformation equations and the dynamic equations, this study calculates piezoelectric forces and velocity of the moving body. These theoretical results are validated by experimental results.

3.1. Deformation of piezoelectric buzzer

Assuming that the rim of a piezoelectric buzzer is fixed but the center can vibrate freely. When the driving voltage is applied to the buzzer, the buzzer center deforms. Piezoelectric deformation arisen from the voltage V is expressed by [25]

$$\delta = NC_eV \tag{1}$$

where N denotes a piezoelectric coefficient and is written as

$$N = \frac{3g_{31}}{4\pi t} \tag{2}$$

where C_e denotes the capacitance of the piezoelectric buzzer and is written as

$$C_e = \frac{2\in_{33}^T \pi r^2}{t} \tag{3}$$

where r is the radius of the piezoelectric buzzer, t is the thickness of the piezoelectric buzzer, and g_{31} and $\in_{33}^T$ respectively denote piezoelectric and dielectric constants of the piezoelectric buzzer. Substituting Eqs. (1) and (2) into (3) yields deformation equation

$$\delta = \frac{3}{2} g_{31} \in_{33}^T \frac{r^2}{t^2} V \tag{4}$$

Fig. 6 shows the direction of both the driving voltage and the deformation of two buzzers. Fig. 6(a) shows the buzzer state without driving voltage. When two buzzers with both positive voltages travel in the same direction, two buzzers generate deformation and force in the same direction. The principle enables the moving body to generate linear displacement, as shown in Fig. 6(b). However, as depicted in Fig. 6(c), if both buzzers with positive and negative

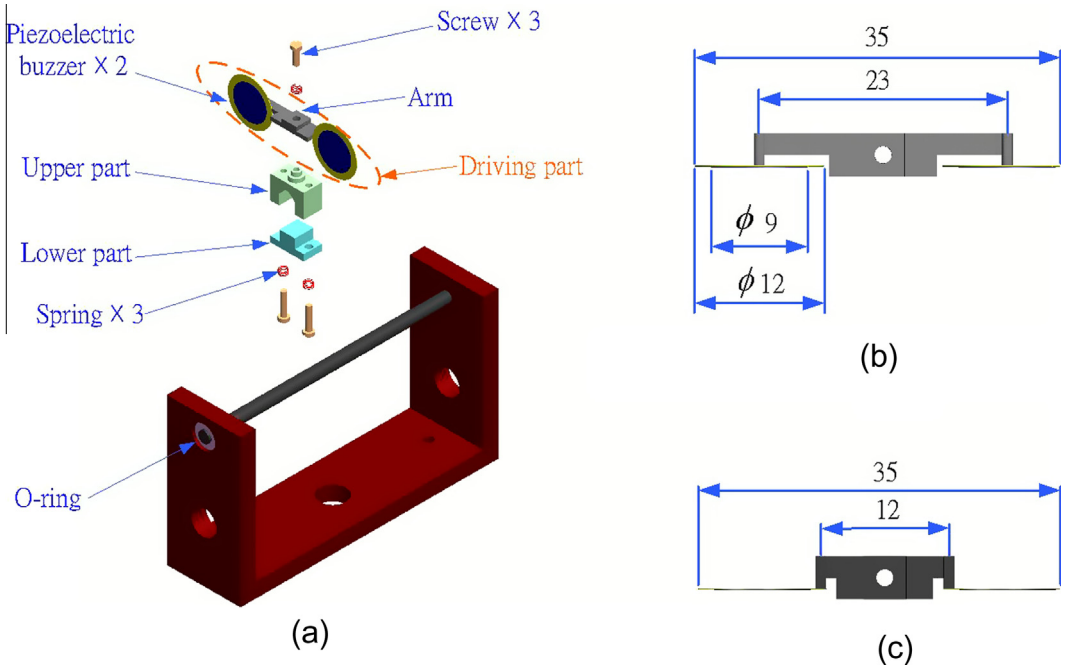

Fig. 3. Exploded view of a 2-DOF piezoelectric actuator and the dimensions of the driving part: (a) exploded view; (b) driving part dimensions in mm of type-A actuator; and (c) driving part dimensions in mm of type-B.

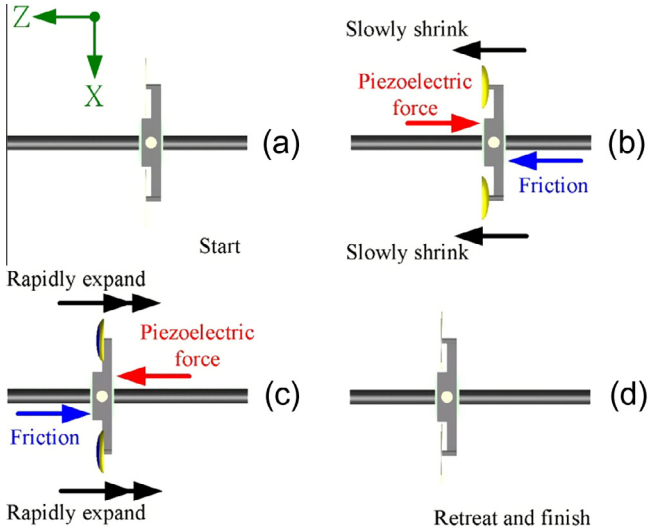

Fig. 4. Principle of actuator translation: (a) the moving body is initially stationary. (b) When both piezoelectric buzzers slowly shrink, the moving body does not produce motion and remains in its original location. (c) When the piezoelectric buzzers rapidly expand, the piezoelectric force triggers motion of the moving body. (d) Both buzzers return to their undeformed state.

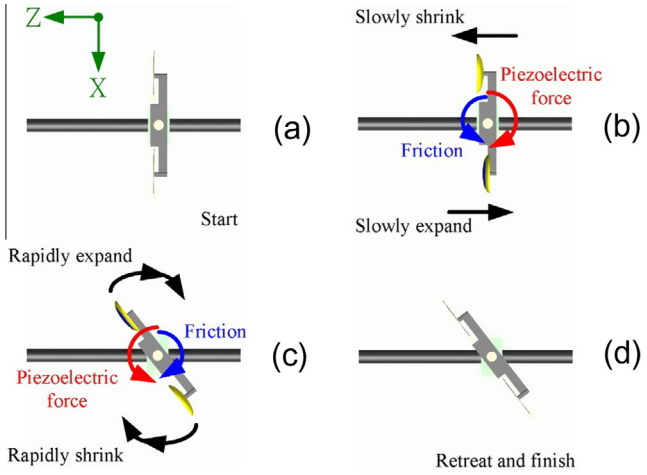

Fig. 5. Principle of actuator rotation motion: (a) the moving body is initially stationary. (b) When the top buzzer slowly shrinks while the bottom buzzer slowly expands, the piezoelectric force is too small to move the moving body. (c) When the top buzzer rapidly expands while the bottom buzzer rapidly shrinks, generated torque enables the moving body to rotate counterclockwise. (d) Finally, the two piezoelectric buzzers returned to their undeformed state.

voltages are traveling in opposite directions, both buzzers generate deformation and forces in opposite directions, which cause the moving body shown in Fig. 5(c) to rotate.

3.2. Equation of motion

The mechanical model of piezoelectric actuator can be simplified as shown in Fig. 7. As the voltage is applied to piezoelectric buzzers, piezoelectric buzzers rapidly produce a left deformation, making the piezoelectric buzzers produce a force to the right. When a dynamic friction occurs between the rod and the moving body, the moving body moves to the right. According to Newton's second law, the dynamic equation is written as

$$(2m_p + m_m)\ddot{x}_1 + 2c_p\dot{x}_1 + 2k_p x_1 = F_p - F_f \tag{5}$$

The piezoelectric equation, strain, curvature, and stress of piezoelectric buzzers are respectively written as [26,27]

$$\varepsilon = S_{11}\sigma + d_{31}\frac{V}{t} \tag{6}$$

$$\varepsilon_1 = tk_r - \frac{V}{t}d_{31} \tag{7}$$

$$k_r = 3g_{31}\epsilon_{33}^{T}\frac{V}{t^2} \tag{8}$$

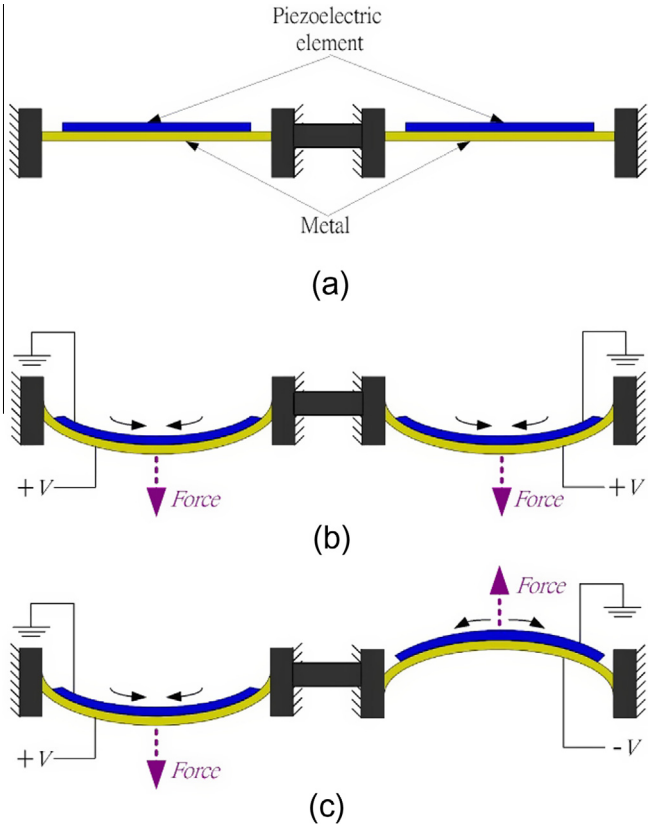

Fig. 6. Driving voltage and deformation direction of two piezoelectric buzzers: (a) subject to zero voltage; (b) subject to both positive voltage; and (c) subject to positive and negative voltages, respectively.

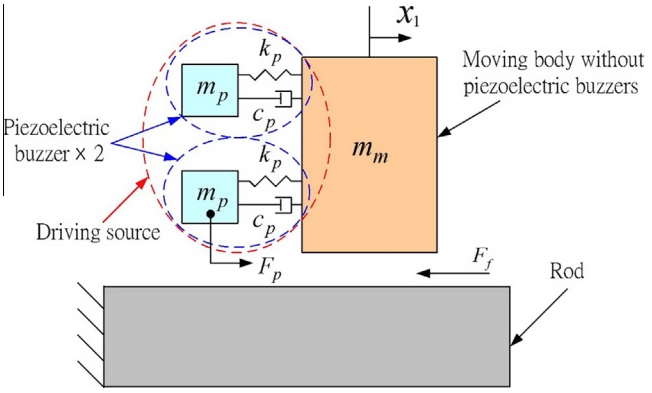

Fig. 7. Mechanical model of the present piezoelectric actuator.

$$\sigma = \frac{F_p}{A} \tag{9}$$

where m_p is the mass of the piezoelectric buzzer, m_m is the mass of the moving body without piezoelectric buzzers, k_p is the stiffness coefficient of the piezoelectric buzzer, c_p is the damping coefficient of the piezoelectric buzzer, F_p is the force applied to the moving body, F_f is the friction force, $\ddot{x}_1$ is the acceleration of the moving body, $\dot{x}_1$ is the velocity of the moving body, x_1 is the displacement of the moving body, ε is the strain of the piezoelectric buzzer, σ is the stress of the piezoelectric buzzer, S_{11} is the elasticity constant of the piezoelectric buzzer, d_{31} is the charge constant of the piezoelectric buzzer, k_r is the curvature of the piezoelectric buzzer, and A is the buzzer disk area.

The term ε_1 in Eq. (7) denotes the strain of piezoelectric buzzer. The total strain is obtained by multiplying ε_1 by 2 because the driving source is composed of two same piezoelectric buzzers. Based on Eqs. (6) and (7), the piezoelectric equation is rewritten as

$$\frac{2V}{t}(3g_{31}\in_{33}^{T} - d_{31}) = S_{11}\frac{F_p}{A} + d_{31}\frac{V}{t} \tag{10}$$

Rearranging Eq. (10) gives the driving source force

$$F_p = \frac{3AV}{S_{11}t}(2g_{31}\epsilon_{33}^{T} - d_{31}) \tag{11}$$

Combining Eqs. (11) and (1) leads to the system dynamic equation

$$(2m_p + m_m)\ddot{x}_1 + 2c_p\dot{x}_1 + 2k_p x_1 = \frac{3AV}{S_{11}t}(2g_{31}\epsilon_{33}^{T} - d_{31}) - F_f \tag{12}$$

The friction term [28] is assumed to have the following non-linear parametric form

$$F_f(\dot{x}_1) = \gamma_1(\tanh(\gamma_2\dot{x}_1) - \tanh(\gamma_3\dot{x}_1)) + \gamma_4\tanh(\gamma_5\dot{x}_1) + \gamma_6\dot{x}_1 \tag{13}$$

where the friction in Eq. (13) has the following properties. The static coefficient of friction can be approximated by $\gamma_1 + \gamma_4$. The term $\tanh(\gamma_2\dot{x}_1) - \tanh(\gamma_3\dot{x}_1))$ captures the Stribeck effect where the friction coefficient decreases from the static coefficient of friction with increasing slip velocity near the origin. A viscous dissipation term is given by $\gamma_6\dot{x}_1$. The Coulomb friction coefficient is present in the absence of viscous dissipation and is modeled by the term $\gamma_4\tanh(\gamma_5\dot{x}_1)$.

Since this study uses Eq. (13) in simulation as the friction model, six parameters have to be identified. γ_4 and γ_5 account for the Coulomb effect and are thus critical. Values of parameters γ_1–γ_5 in this study are firstly adopted from reference [28], and then γ_4 and γ_5 are fine-tuned until simulation and experimental curves match. γ_6 accounts for viscous friction [28]. Hence, in this piezoelectric actuator study without lubricant between the moving body and rod, parameter γ_6 is set to an extremely small value to minimize γ_6 influence on the friction model.

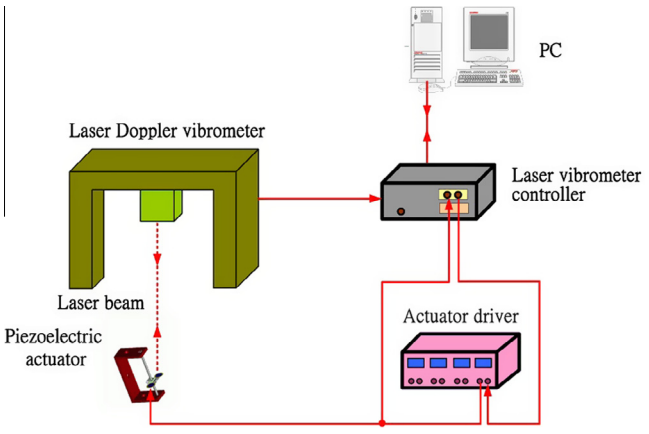

Fig. 8. Experimental setup for actuator frequency response.

4. Experimental results and discussion

4.1. Dynamic analysis in term of frequency response

Dynamic analysis using frequency response is conducted to investigate piezoelectric buzzer characteristics and identify resonance frequencies before selecting a resonant frequency for driving the moving body. Exciting buzzers at resonant frequency enables the moving body to move at high speeds. Fig. 8 shows the experimental setup of the system identification. The equipment used for the experiment includes a personal computer, laser vibrometer controller, laser Doppler vibrometer, and actuator driver (Echo ENP-4012B).

The driving voltage is a 2 V sinusoidal wave within the scanning range of 10–20 kHz. The driving voltage of the actuator driver is adjusted to drive the moving body on the piezoelectric actuator. The vibrometer emits laser beams to detect the vibration displacement of the piezoelectric buzzer, passing the signal value of the vibration displacement to the vibrometer controller. Finally, vibration data stored in the vibrometer controller are converted into Bode diagrams.

Corresponding to Fig. 1 that shows photographs of types A and B actuators, Fig. 9 depicts their Bode diagrams, where resonant frequencies of type-A include 3036 Hz, 3377 Hz, and 7445 Hz and those of type-B are 396 Hz, 536 Hz, and 6900 Hz. The vibration mode shape of type-A at the first natural frequency is symmetric and synchronized on the circumference; therefore the first natural frequency is suitable for driving frequency. For type-B the mode shapes at the first and the second frequencies are not easy to be symmetrical and synchronized despite the large deformation of the buzzers. Thus, neither the first nor the second frequency is proper for being a driving frequency. Although the deformation of the third natural frequency is smaller than those of the first and second frequencies in type-B, the third frequency is suitable for driving due to the synchronized vibrations on the circumference. According to Fig. 9, the mode shape, support type and the natural frequency are mutually affected. The advantages of

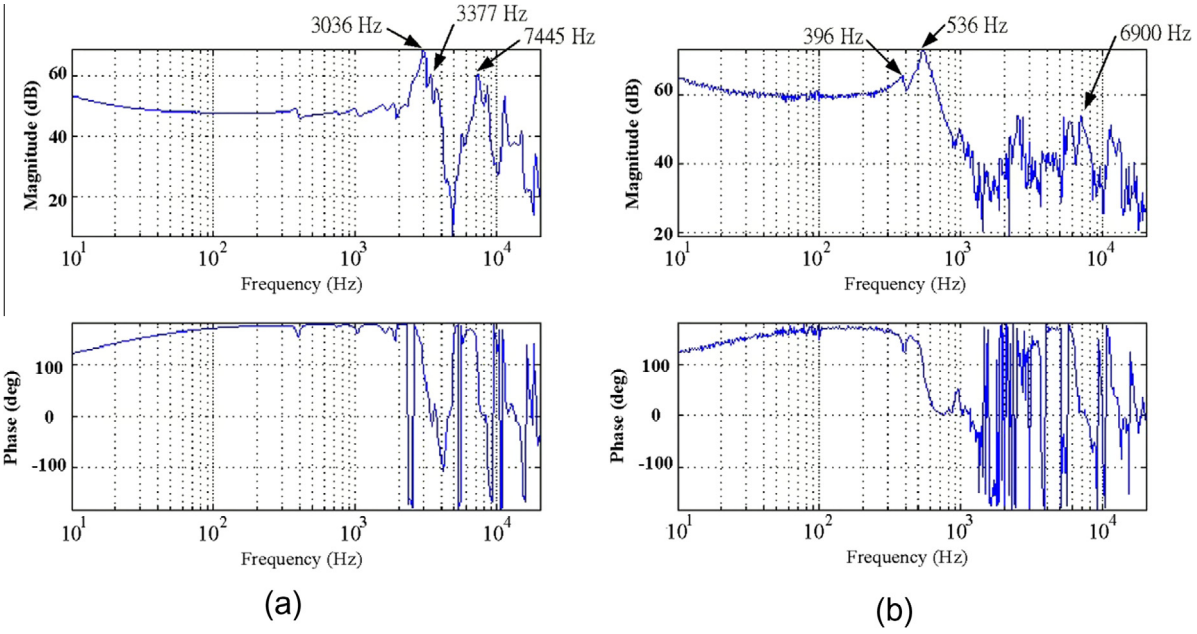

Fig. 9. Bode diagrams of (a) type-A and (b) type-B actuators.

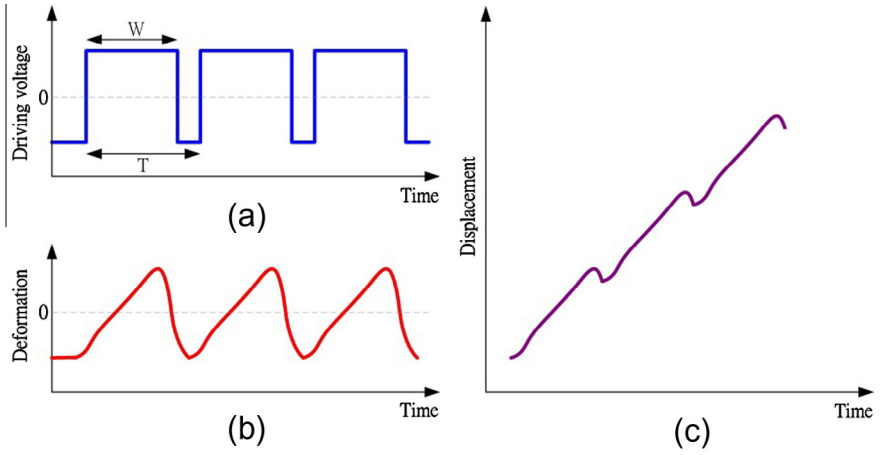

Fig. 10. Schematic diagrams of (a) driving voltage with duty ratio = W/T, (b) deformation of piezoelectric buzzer in actuator, and (c) actuator displacement.

type-A and type-B are the good stability and wide work range, respectively.

4.2. Performance measurement

Velocity measurements, angular velocity measurements, and force measurements experiments are carried out for comparison between actuators of types A and B. According to resonant peaks, driving frequencies selected for both actuators are 3036 HZ and 6900 Hz, respectively. When the driving voltage employs rectangular waves [20,21] to drive the piezoelectric buzzer, according to the excitation frequency, frequency response of piezoelectric buzzer, and duty ratio of the driving voltage, the piezoelectric buzzer deforms and produces an output wave resembling a sawtooth wave. The duty ratio of the driving voltage rectangular waveforms is used in this study to control the sawtooth proportion and the sawtooth wave direction. Changes in the duty ratio influence the movement direction and velocity.

Fig. 10 shows a schematic diagram of the driving voltage, buzzer deformation, and actuator displacement. As depicted in Fig. 10(b), in each period of the sawtooth signal, the slope of the first half is smaller than that of the second half. Therefore, in the first half, the static friction exists between the moving body and the rod, and no relative displacement occurs between both. In the second half, however, the slope is larger, and the dynamic friction between the moving body and rod allows the moving body to move for a short distance. As a consequence, persistent switching between static and dynamic friction causes the moving body to move, as shown in Fig. 10(c).

For the actuator velocity measurement, Fig. 11 shows the experimental setup, which includes a vibrometer controller (Polytec OFV 3001), vibrometer (Polytec OFV 512), waveform generator (Agilent 33210A), and actuator driver (Echo ENP-4012B). In experiments, firstly, the waveform generator is used to generate the rectangular voltage waveform with a duty ratio. The driving voltage of the actuator driver is adjusted so as to drive the actuator. The vibrometer is used to measure the actuator displacement and velocity, which are in turn transmitted to the vibrometer controller.

Under proper combinations of the driving voltage and the duty ratio, the piezoelectric buzzers generate different piezoelectric forces and deformation velocity, finally producing the displacement of the moving body. Experimental and simulation results of velocity variation with duty ratios are depicted in Fig. 12, in which the driving voltage is 40 V for both actuators and driving frequencies are 3036 HZ and 6900 Hz for types A and B, respectively. When the duty ratio is prescribed as 50%, the buzzer deforms in an isosceles triangle waveform, the moving velocity of the moving body is difficult to control and stabilize; thus, a duty ratio of 50% is not appropriate. According to experiments, 10% and 90% duty ratios have little effect on velocity; thus, results of both duty ratios are not included in comparison. Fig. 12 also shows that when the duty ratio is 20–40% and 60–80%, the moving bodies moved in opposite directions. The fastest speed is obtained at duty ratios of 40% and 60%. Type-A actuator moves faster than type-B. Type-A simulation results are consistent with experimental results of type-A since equations of motion are derived based on type-A geometry.

Concerning rotational motion of actuators, Fig. 13 shows that the measured angular velocity of type-A is faster than type-B. Unbalanced weights on both sides of the rotational arm, as shown in Fig. 3(a), result in the angular velocity discrepancy between simulation and experimental results. The maximum rotation angle in the *Y*-axis direction, which is depicted in Figs. 1 and 2, can reach 270° in experiments.

Fig. 14 depicts an open-loop control block diagram in experiments. Table 1 compares the performances of the proposed design and the literature. Compared performances include measured velocity, angular velocity, and force. According to Table 1, the present design generates faster velocity while smaller force than the literature. Its piezoelectric material thickness of mere 0.13 mm results in small force generation.

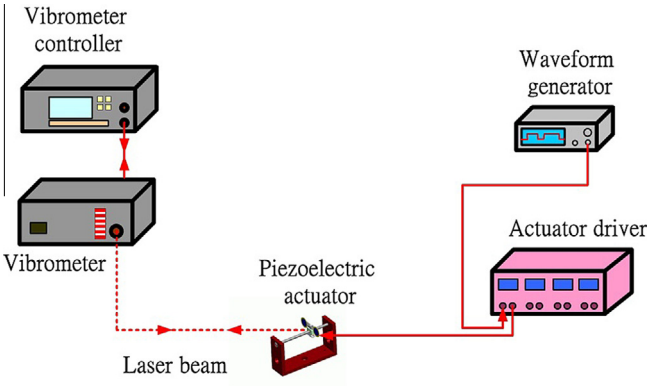

Fig. 11. Experimental setup for the actuator velocity measurement.

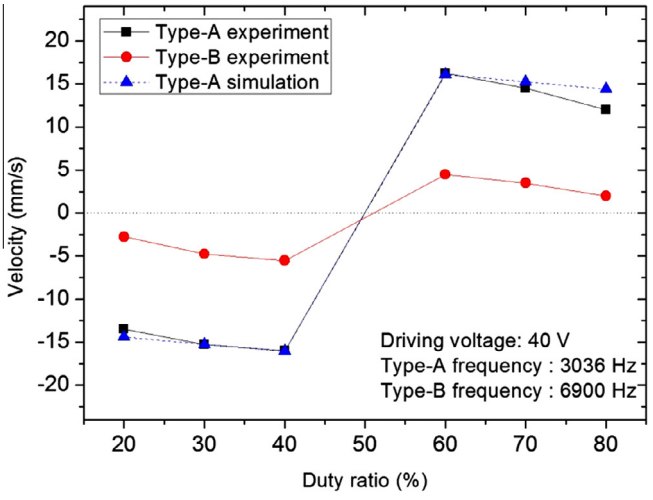

Fig. 12. Comparison of experimental and simulation results in velocity variation with duty ratios.

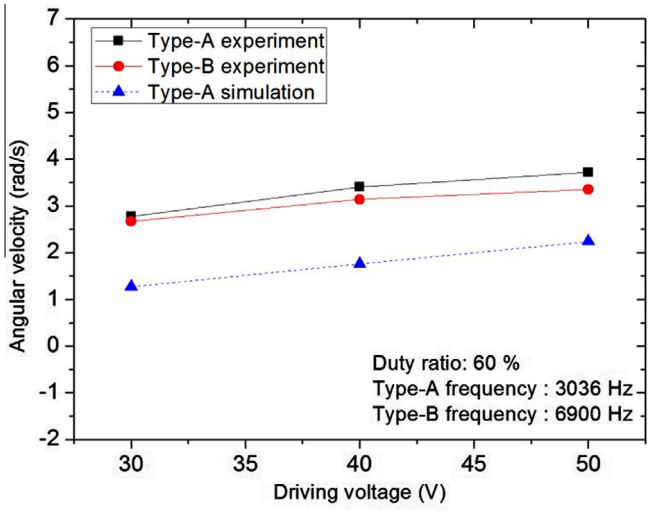

Fig. 13. Comparison of experimental and simulation results in angular velocity.

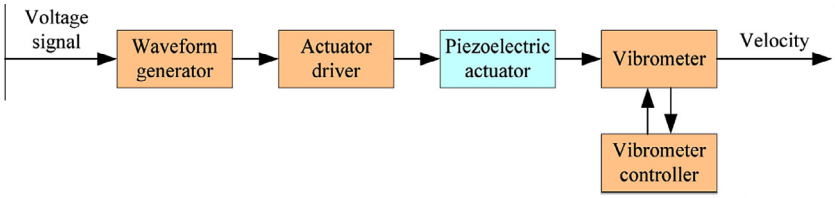

Fig. 14. Open-loop control block diagram in experiments.

Table 1
Comparison of the present actuator performance with the literature.

Author	Dimensions of piezoelectric (mm)	Voltage frequency	Velocity (mm/s)	Angular velocity (rad/s)	Force (mN)
This study	Φ9 × t0.13 (2 pieces)	50 V 3.036 kHz	21	3.72	2.32
Liu et al. [8]	Φ5 × t0.18 (2 pieces)	50 V 1.1 kHz	3.5	N/A	88
Jun et al. [9]	Φ10.8 × t0.84 (1 piece)	80 V 36.5 kHz	4	N/A	80
Kawakita et al. [13]	Φ8 (6 pieces)	40 V 2 kHz	5.9	N/A	100
Zhang et al. [14]	40 × 20 × 0.4 (4 pieces)	90 V 0.013 kHz	0.083	0.0033	2000
Yoshida et al. [21]	Φ1.2 × t2.5 (1 piece)	3 V 150 k Hz	14.3	N/A	65
Morita et al. [22]	5 × 2 × 0.2 (1 piece)	40 V 576 kHz	N/A	41.88	N/A
Ko et al. [29]	Φ3 × t0.1 (2 pieces)	40 V 63 kHz	8	N/A	120
Mashimo et al. [30]	14 × 10 × 0.5 (4 pieces)	42 V 78.5 kHz	95	15.7	330
Lim et al. [31]	Φ28 × t2 (2 pieces)	20 V 92 kHz	N/A	20.94	N/A

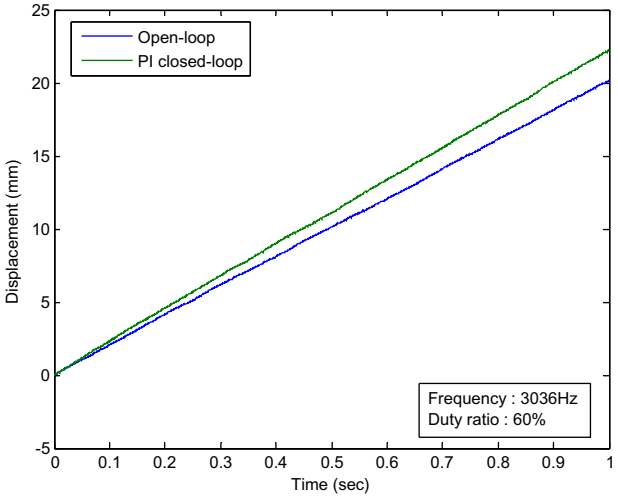

Fig. 15. Displacement curves resulting from PI control and open-loop control.

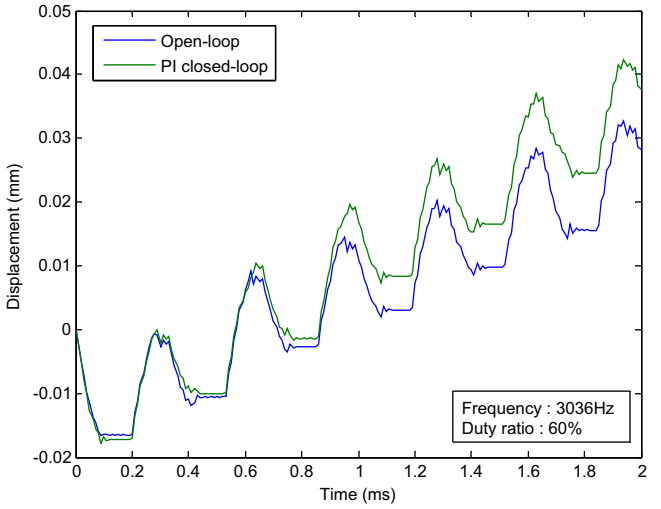

Fig. 16. Displacement curves enlarged from Fig. 15 within 2 ms resulting from PI control and open-loop controls.

This study has compared performances of actuators subjected to open-loop control and proportional-integral (PI) closed-loop control by using the Matlab/Simulink software. Fig. 15 compares both displacement curves of PI control and open-loop control. Under PI control, the displacement reaches 22.2 mm within 1 s while the open-loop displacement is 20.1 mm. Accordingly, PI control increases velocity by 10%.

In order to observe more closely, Fig. 16 further depicts displacement curves within 2 ms in Fig. 15. It is found from Fig. 16 that the backward displacement of the moving body becomes smaller when the actuator is under PI control rather than open-loop control. This smaller backward displacement results in the velocity increase of the moving body.

5. Conclusion

This study has designed and measured innovative 2-DOF piezoelectric actuators, alternately subjected to piezoelectric force and dry friction, which not only are capable of translation but also rotation. Compared with the literature, the present new piezoelectric

actuator design achieves both 1-DOF translational and 1-DOF rotational motions. According to experimental results, the present actuator can accomplish the translational velocity of 21 mm/s, angular velocity of 3.72 rad/s, and 2.32 mN in force. According to experimental results concerning velocities, angular velocities, and forces, type-A performs better than type-B because the type-A design leads to larger forces and faster moving velocity. Fig. 9 depicts that the bandwidth of type-A actuator is much larger than that of type-B actuator. Accordingly, the system response of type-A actuator indeed should be much faster than that of type-B actuator. The proposed dynamic model that incorporates both mechanical and piezoelectric properties is validated by experimental results.

References

[1] Watson B, Friend J, Yeo L. Piezoelectric ultrasonic micro/milli-scale actuators. Sens Actuators, A 2009;152(2):219–33.

[2] Wang C-K, Huang H-P, Chien K. Piezo-electric driver of ultrasonic motor on the humanoid robot. In: IEEE international conference on advanced robotics and its social impacts; 2008. p. 23–5.

[3] Uchino K. Piezoelectric actuators 2006. Springer J Electroceram 2007;20(3–4):1–11.

[4] Bansevicius R, Blechertas V. Multi-degree-of-freedom ultrasonic motors for mass-consumer devices. J Electroceram 2007;20(3-4):1–4.

[5] Morita T. Miniature piezoelectric motors. Sens Actuators, A 2003;103(3):291–300.

[6] Zhang ZM, An Q, Li JW, Zhang WJ. Piezoelectric friction–inertia actuator – a critical review and future perspective. Springer Int J Adv Manuf Technol 2012;62(5-8):1–7.

[7] Uchino K, Giniewicz JR. Micromechatronics. Marcel Dekker; 2003. p. 3–7.

[8] Liu P-K, Wen Z-J, Sun L-N. An in-pipe microrobot actuated by piezoelectric. Springer Chinese Sci Bull 2009;54(12):2134–42.

[9] Jun S-H, Lee S-M, Lee S-H, Kim H-E, Lee K-W. Piezoelectric linear motor with unimorph structure by co-extrusion process. Sens Actuators, A 2008;147(1):300–3.

[10] Li J, Sedaghati R, Dargahi J, Waechter D. Design and development of a new piezoelectric linear Inchworm actuator Original. Mechatronics 2005;15(6):651–81.

[11] Kim J, Kang B. Micro–macro linear piezoelectric motor based on self-moving cell. Mechatronics 2009;19(7):1134–42.

[12] Mazeika D, Vasiljev P. Linear inertial piezoelectric motor with bimorph disk. Mech Syst Signal Process 2013;36(1):110–7.

[13] Kawakita S, Isogai T, Ohya N, Kawahara N. Multi-layered piezoelectric bimorph actuator. In: IEEE international symposium on micromechatronics and human science; 1997. p. 73–78.

[14] Zhang H-Z, Cheng G-M, Zhao H-W, Zeng P, Yang Z-G. A 2-dimensional impact driven precise actuator using piezoelectric bimorphs. Springer Frontiers Electrical Electron Eng 2006;1(4):405–9.

[15] Pozzi M, King T. Piezoelectric modelling for an impact actuator. Mechatronics 2003;13(6):553–70.

[16] Belly C, Charon W. Benefits of amplification in an inertial stepping motor. Mechatronics 2012;22(2):177–83.

[17] Ko H-P, Lee K-J, Yoo K-H, Kang C-Y, Kim S, Yoon S-J. Analysis of tiny piezoelectric ultrasonic linear motor. Jpn J Appl Phys 2006;45(5B):4782–6.

[18] Ko H-P, Kim S, Borodinas SN, Vasiljev PE, Kang C-Y, Yoon S-J. A novel tiny ultrasonic linear motor using the radial mode of a bimorph. Sens Actuators, A 2006;125(2):477–81.

[19] Lim K-J, Lee J-S, Park S-H, Kang S-H, Kim H-H. Fabrication and characteristics of impact type ultrasonic motor. J Eur Ceram Soc 2007;27(13–15):4159–62.

[20] Kang C-Y, Yoo K-H, Ko H-P, Kim H-J, Ko T-K, Yoon S-J. Analysis of driving mechanism for tiny piezoelectric linear motor. J Electroceram 2006;17(2–4):609–12.

[21] Yoshida R, Okamoto Y, Okada H. Development of smooth impact drive mechanism. Jpn Soc Precision Eng 2002;68(4):536–41.

[22] Morita T, Murakami H, Yokose T, Hosaka H. A miniaturized resonant-type smooth impact drive mechanism actuator. Sens Actuators, A 2012;178:188–92.

[23] Takuma N, Hiroshi H, Takeshi M. Resonant-type smooth impact drive mechanism (SIDM) actuator using a bolt-clamped langevin transducer. Ultrasonics 2012;52(2):75–80.

[24] Hunt J, Bhushan B. Device level studies of adaptive optics sliding components in microprojectors. Springer Microsyst Technol 2012;18(1):137–48.

[25] Spencer WJ, Corbett WT, Dominguez LR, Shafer BD. An electronically controlled piezoelectric insulin pump and valves. IEEE Trans Son Ultrason 1978;25(3):153–6.

[26] Ling S-F, Du H, Jiang T. Analytical and experimental study on a piezoelectric linear motor. Smart Mater Struct 1998;7(3):382–8.

[27] Deshpande M, Saggere L. An analytical model and working equations for static deflections of a circular multi-layered diaphragm-type piezoelectric actuator. Sens Actuators, A 2007;136(2):673–89.

[28] Makkar C, Dixon WE, Sawyer WG, Hu G. A new continuously differentiable friction model for control systems design. In: IEEE/ASME international conference on advanced intelligent, mechatronics; 2005. p. 600–605.

[29] Ko P-H, Kang C-Y, Kim J-S, Borodin SN, Kim S, Yoo S-J. Constructions and characteristics of a tiny piezoelectric linear motor using radial mode vibrations. J Electroceram 2006;17(2–4):603–8.

[30] Mashimo T, Toyama S, Matsuda H. Development of rotary-linear piezoelectric actuator for mri compatible manipulator. In: IEEE/RSJ international conference on intelligent robots and systems acropolis convention center; 2008. p. 113–118.

[31] Lim K-J, Park S-H, Yun Y-J, Lee K-Y, Kang S-H, Lee J-S, et al. Characteristics of disk-type linear ultrasonic motor for application to *x*–*y* stage. J Electrical Eng Technol 2006;1(1):101–5.